EUROPEAN ORGANIZATION FOR NUCLEAR RESEARCH

CHARGED PARTICLE PRODUCTION AND CORRELATIONS
AT HIGH TRANSVERSE MOMENTUM AT THE CERN INTERSECTING STORAGE RINGS

Brookhaven[1]-CERN[2]-Copenhagen[3]-Lund[4]- Pennsylvania[5]-
Rutherford[6]- Tel Aviv[7] Collaboration

T. Åkesson[2], M.G. Albrow[6], S. Almehed[4], O. Benary[7], H. Bøggild[3],

O. Botner[3], H. Brody[5], V. Burkert[2a], D. Cockerill[6], S. Dagan[7],

E. Dahl-Jensen[3], I. Dahl-Jensen[3], P. Dam[3], G. Damgaard[3], G. von Dardel[4],

W.M. Evans[6], C.W. Fabjan[2], P. Frandsen[2], S. Frankel[5], W. Frati[5],

M.D. Gibson[6], H. Gordon[1], A. Hallgren[2b], K.H. Hansen[3], B. Heck[2],

S. Henning[4c], J.W. Hiddleston[6], H.J. Hilke[2], J.E. Hooper[3], G. Jarlskog[4],

P. Jeffreys[6], T. Jensen[2d], G. Kesseler[2], T. Killian[1e], J. van der Lans[2],

J. Lindsay[2], D. Lissauer[7], E. Lohse[3], B. Lörstad[4], T. Ludlam[1],

N.A. McCubbin[6], A. Melin[4f], U. Mjörnmark[2], W. Molzon[5], R. Møller[3],

B.S. Nielsen[2], S.Ø. Nielsen[3g], A. Nilsson[4h], L.H. Olsen[3], Y. Oren[7],

L. Rosselet[2i], E. Rosso[2], A. Rudge[2], R.H. Schindler[2j], B. Schistad[3k],

W.J. Willis[2], M. Winik[1m], W. Witzeling[2] and C. Woody[1]

The Axial Field Spectrometer Collaboration

1) Brookhaven National Laboratory, Upton, NY, USA.
2) CERN, Geneva, Switzerland.
3) Niels Bohr Institute, Copenhagen, Denmark.
4) University of Lund, Sweden.
5) University of Pennsylvania, Philadelphia, Pa., USA.
6) Rutherford Appleton Laboratory, Didcot, UK.
7) University of Tel Aviv, Israel.
Present addresses:
a) Physikalisches Institut, Universität Bonn, Fed. Rep. Germany.
b) University of Uppsala, Sweden.
c) Airglass AB, Sjöbo, Sweden.
d) Cornell University, Ithaca, NY, USA.
e) Bell Laboratories, Murray Hill, NJ, USA.
f) Soft Start AB, Kyrkheddinge, Sweden.
g) RECKU, Copenhagen, Denmark.
h) DESY, Hamburg, Fed. Rep. Germany.
i) University of Geneva, Switzerland
j) California Institute of Technology, Calif., USA.
k) C.Rovsing A/S, Copenhagen, Denmark
m) Weizmann Inst. of Science, Rehovot, Israel.

ABSTRACT

We study the production of identified charged particles in pp colli-
sions at a c.m. energy of 63 GeV in events with an identified high-p_T
trigger particle. The measurements were performed at the CERN Intersecting
Storage Rings using the Axial Field Spectrometer.

Production ratios are presented as a function of p_T in the range
2.5 to 8 GeV/c.

The charge compensation in the hemisphere containing the high-p_T
trigger particle depends strongly on the identity of the trigger particle,
and on that of the associated particles.

The positive to negative ratio of away-side particles depends on the
trigger particle identity, but in all cases it rises with the p_T of these
particles.

A comparison with the predictions of the Lund model shows that this
model can account for all the qualitative trends of the data. However, the
particle ratios as a function of p_T and the production of protons and
antiprotons are not well reproduced. The data on correlations with protons
suggest a more elaborate mechanism for baryon production.

1. **INTRODUCTION**

We report on measurements of identified charged particles produced in pp collisions at a c.m. energy of 63 GeV with an identified charged particle at high p_T emitted in the central region.

The composition of charged particles up to $p_T \sim 8$ GeV/c is measured. Previous data on identified particles at this collision energy are limited to $p_T < 2.5$ GeV/c (British-Scandinavian (BS) Collaboration [1]) or cover more forward angles (Ames-Bologna-CERN-Dortmund-Heidelberg-Warsaw (ABCDHW) and CERN-Dortmund-Heidelberg-Warsaw (CDHW) Collaborations [2]).

Charge correlations between an identified high-p_T particle and associated identified charged particles are also studied. Such data are sensitive to detailed questions of quantum number correlations in jet fragmentation. Similar measurements have been reported by the BFS Collaboration [3] and the CDHW collaboration [4]. However the associated particles were not identified in either of these previous studies. In particular our results are compared with the Lund model [5], where the parton-parton interactions are calculated in lowest-order perturbative QCD. In this model the fragmentation of the colour strings has been tuned to describe particle production in e^+e^- interactions.

In hadronic collisions the requirement of a high-p_T particle is expected to select parton-parton interactions. The quantum numbers of the primary parton are likely to be found in the leading high-p_T particle. The charge of this particle is normally compensated locally as a result of quark-antiquark pair creation, and therefore short-range correlations which depend on the nature of the trigger particle can be expected.

Furthermore, as the proton contains one d and two u valence quarks, a scattered valence quark is more often a u quark, implying more leading

positives than negatives both on the trigger side and on the away side. In pp collisions, long-range charge correlations can arise from the uud valence quark content of the proton, and from the two-gluon annihilation process $gg \rightarrow q\bar{q}$. The Lund model predicts that this latter process will contribute less than 1% in our case. (More subtle long-range correlations can arise in special kinematic configurations as studied by the CDHW group [4].)

This paper is organized as follows. Section 2 describes the apparatus and data analysis. In Section 3 the inclusive particle production is studied in terms of ratios between identified particles. Section 4 describes our investigation of the charge compensation versus rapidity along the jet axis, given essentially by the trigger particle. In Section 5 we study the associated production of protons and antiprotons, and in Section 6 the various aspects of away-side correlations with the trigger particle.

2. APPARATUS AND DATA ANALYSIS

This experiment was performed at the CERN Intersecting Storage Rings (ISR) using the Axial Field Spectrometer (AFS) in its Cherenkov arm configuration, as shown in Fig. 1 in a view transverse to the colliding beams. The apparatus and its performance are described in detail elsewhere [6]. Here we mention briefly only those components of the apparatus which were used in the present investigation.

The central cylindrical drift chamber is 1.4 m long and extends radially from 0.2 to 0.8 m. It is segmented azimuthally in 4° sectors, each with 42 sense wires. It provides full 2π coverage in azimuth except for two 16° wedges above and below the interaction region. It is situated

in an axially symmetric magnetic field of 0.5 T. Position coordinates in the plane transverse to the sense wires are determined by drift time with a resolution of 230 µm. The position along the wires, parallel to the beams, is found from the pulse heights measured at the two ends of the wires. The corresponding resolution is ~1.5 cm. The over-all momentum resolution is dp/p ~ $\sqrt{[(0.025\ p)^2 + (0.01)^2]}$ (p in GeV/c), where the first term comes from measurement errors, and the second term from multiple scattering in the chamber. The pulse-height measurements also provide dE/dx information used for particle identification. This gives pion identification in the momentum range 0.2 to 0.5 GeV/c, kaon identification in the momentum range 0.3 to 0.7 GeV/c, and proton identification in the momentum range 0.4 to 1.1 GeV/c.

Three sets of threshold Cherenkov counters subtend an azimuthal angle of 45° and 45° < θ < 135° in polar angle. The Cherenkov counter closest to the drift chamber -- the aerogel Cherenkov counter -- consists of 88 cells arranged in 4 layers in depth. The cells are read out using wavelength-shifter bars. The average number of detected photoelectrons per cell from a β ~ 1 particle is only 0.3 as determined from data. For the full 88-cell counter the probability for a track to give at least one photoelectron is around 60%. On the other hand, 20% of the tracks with momentum below the pion threshold (0.5 GeV/c) have associated noise in the counter (fig. 2). In this study the aerogel counter is used to identify pions in the momentum range 0.5 to 2.0 GeV/c.

The second Cherenkov counter, containing Freon-12 at 4 atm, is subdivided into 12 optical cells. The average number of photoelectrons produced by a β ~ 1 particle is 20. The performance of the detector is illustrated in fig. 3. It allows pion/heavy particle separation for

$1.5 < p_{lab} < 5.3$ GeV/c. After appropriate cuts the identified heavy-particle sample is quite clean, whereas the pion sample has a contamination from heavier particles of ~1.5%, mainly due to overlapping γ-conversions from π^0 decays.

The third Cherenkov counter contains Freon-12 at atmospheric pressure, and comprises 18 optical cells. The average number of photo-electrons for a β ~ 1 particle is ~10, giving a good separation of different particle identities, (fig. 4.) Together with the high-pressure counter, it provides pion, kaon, and proton separation for $p_{lab} > 5.5$ GeV/c.

Copper calorimeters placed behind the atmospheric pressure counters cover 14% of the solid angle of these counters. These calorimeters were installed to provide a cross-check of the momentum measurement at $p_{lab} > 8$ GeV/c, and were used in the trigger for part of the data sample.

Two sets of multiwire proportional chambers (MWPCs) placed between the Cherenkov counters cover the same solid angle as these counters.

Interactions resulting in the production of a high-p_T charged particle within the solid angle of the Cherenkov counters were selected using a three-level trigger. The first level uses the scintillator hodoscope, which surrounds the beam pipe, together with groups of wires in the MWPCs to require $p_T > 0.8$ GeV/c. The second level uses hits from individual wires of the MWPCs. The third level uses a microprocessor, ESOP, which finds track candidates from a set of the drift chamber signals selected by the lower level triggers, and estimates track momentum from the curvature in the magnetic field. The trigger threshold for these data was set to p_T ~ 5 GeV/c. The experiment relies heavily on ESOP to reduce background from false pretriggers, and the sensitivity is increased by a factor of between 200 and 750 compared with the second-level trigger. Details have been given elsewhere [7].

The events were first processed through the AFS drift chamber reconstruction and fitting programs [8]. Events were accepted if they contained a reconstructed primary vertex, a condition fulfilled by 99% of the events. Cuts were imposed on the tracks to ensure that they belonged to the event and that their momenta were reasonably well determined. All tracks were transformed to the centre-of-mass system, using the pion mass if the particle was not identified as a kaon or proton. Cuts on associated particles restricted them to be within ± 0.8 in rapidity and in the range $0.2 < p_T < 5$ GeV/c. Data were collected with both polarities of the magnetic field, and for associated particles the acceptance is checked to be charge independent. Tracks within the acceptance of the Cherenkov counters were refitted using both drift chamber information and the reconstructed space points in the MWPCs. This procedure served to reject false high-p_T tracks, to reject particles interacting in the material of the Cherenkov counters, and to improve the momentum resolution to $\Delta p/p \sim 10\%$ at $p = 10$ GeV/c.

The final data sample contains 75,500 events, out of which 52,750 have a trigger particle identified as π and 22,750 as a heavy particle. The p_T of the trigger particle was required to be larger than 3 GeV/c, resulting in a mean p_T of 4.1 GeV/c. For p_{lab} above 5.3 GeV/c, 3000 heavy triggers are separated into kaons and protons.

3. PARTICLE COMPOSITION

The fractional composition of the particle flux is shown in fig. 5a for positive particles and in fig. 5b for negative particles. Below 5 GeV/c only pions are identified. The data are averaged over the c.m.s. polar angle interval from 45° to 135° with $\langle \theta \rangle = 90°$ and $\langle |\theta - 90°| \rangle \sim 20°$. We

have not observed a significant variation with θ. For comparison we also show the particle composition at $\langle\theta\rangle \sim 50°$ derived from the invariant cross-sections measured by the CDHW Collaboration [2], and an extrapolation of the fit of the data at lower p_T's from the BS Collaboration (table 4 in ref. 1).

Our data have been corrected for contamination of the pion sample by heavier particles (a correction of 1.5% for $p_T < 5$ GeV/c), for nuclear absorption and particle decays (corrections of 0.5-3%), and for a slightly worse acceptance for protons than for pions and kaons at $p_T > 5$ GeV/c (corrections about 1%). The errors shown in fig. 5 are statistical only. The systematic errors are estimated to be smaller than the statistical errors.

For positively charged particles we find the same fraction of π^+ as that found by the CDHW Collaboration over the whole p_T range, and similar fractions of K^+ and p. However, for the fraction of π^- we do not observe the rise found by the CDHW Collaboration at $\langle\theta\rangle \sim 50°$ for $p_T > 5$ GeV/c; we find a significantly larger fraction of antiprotons.

In order to compare positive and negative particle production, we need to know the relative trigger acceptance, which is very sensitive to systematic effects. It was calculated using a Monte Carlo program, taking into account the position and shape of the interaction region (the diamond), and the geometry of the inner hodoscopes and of the groups of proportional-chamber wires which enter into the first two levels of the trigger system. Furthermore, multiple scattering, relative positions of the drift chamber and the proportional chambers, and the effects of spatial resolution in the chambers were taken into account. Finally, the effect of the on-line microprocessor trigger condition was included in the program.

The event sample used was obtained under rather different conditions in terms of these parameters. The fact that the +/- ratios, calculated from different runs, were found to be consistent after corrections provided a good check of the acceptance calculations. The residual error from run-to-run systematics is estimated to be around 8%.

Figure 6 shows the +/- ratio versus p_T after correction for these trigger acceptance effects. This ratio is increasing in the interval $4 < p_T < 8$ GeV/c, as expected from a simple quark-parton model in which scattered valence quarks are expected to contribute to a larger par of the cross-section at large p_T.

From the +/- ratio and the particle ratios discussed above, it is possible to calculate the fractional composition of all charged particles versus p_T. This is shown in fig. 7 for the interval 5-8 GeV/c. Our measurements are also given in table 1.

The predictions of the Lund model, with the choice of parameters given in ref. 5, are shown as hatched areas in figs. 6 and 7. The data are not very well described by the model. In fig. 6 we see that the model predicts a substantially larger +/- ratio for $p_T < 7$ GeV/c than that observed in the data. The trigger bias effect, i.e. the tendency to select events where one particle takes most of the parton momentum, makes our data quite sensitive to the detailed behaviour of the fragmentation near $z = 1$. For example we find that increasing the width of the jets in the model results in a significant decrease of the +/- ratio. On the other hand, a change in the mixture of quarks and gluons in the model will also effect the relative frequencies of different particles.

Figure 7 shows that the fraction of proton and antiproton production is larger in the model than in our measurements. A basic assumption in the

model is that a diquark-antidiquark pair can be produced in a colour force field in a way that is similar to the production of a quark-antiquark pair [9]. The ratio (0.075) of diquark-antidiquark pair creation to quark-antiquark pair creation is adjusted to reproduce the baryon production in e^+e^- annihilations.

4. CHARGE COMPENSATION VERSUS RAPIDITY ALONG THE TRIGGER-JET AXIS

We will now investigate how the charge of a high-p_T particle in the trigger-side jet is compensated in different regions of phase space. A similar study has been performed by the CDHW Collaboration at the CERN ISR [4]. Our approach follows that given by the TASSO [10] and PLUTO [11] Collaborations at PETRA.

We will study the charge compensation as a function of rapidity along an axis given by the direction of the trigger-side jet. This axis is found by a jet algorithm [12] using the charged particles with $p_T > 0.3$ GeV/c, and is given, within a few degrees, by the trigger particle direction. As in ref. 11, we define an asymmetry $A(y,y') = 2P(y,y') - 1$, where $P(y,y')$ is the probability that two particles, located at rapidities y and y' along the jet axis, have opposite charges. For no charge compensation P is equal to 0.5 and A is zero. We will study the quantity

$$\tilde{A}(y) = \int_2^5 A(y,y') \cdot \varrho(y,y') dy' / \int_2^5 \varrho(y,y') dy' \ ,$$

which is obtained by weighting the asymmetry $A(y,y')$ with the two-particle density $\varrho(y,y')$ and averaging over all "fast" particles, i.e. particles in the rapidity interval $2 < y' < 5$. An equivalent expression of the function $\tilde{A}(y)$ is

$$\hat{A}(y) = \int_2^5 [\varrho(y,y')_{\text{opp.charge}} - \varrho(y,y')_{\text{same charge}}]dy' / \int_2^5 \varrho(y,y')dy' \ .$$

Thus $\hat{A}(y)$, which is bounded between -1 and +1, measures the strength of the average charge compensation between a pair of particles, one of which (the fast one) has rapidity $2 < y' < 5$, and the other (the associated one) has rapidity y. It is clear from the definition of $\hat{A}(y)$ that acceptance effects are divided out.

Figure 8 displays the single-particle density of the associated particles and the trigger particles as a function of rapidity on the jet axis. We see that the region 2 to 5 in rapidity selects mainly the trigger track. The accumulation at a rapidity of around 4 corresponds to pion triggers which define the jet-axis by themselves. The depletion around 0 in rapidity is due to the lower cut at 0.3 GeV/c in p_T of the associated particles which was used to limit the influence of beam jets.

4.1 Particles identified as pions and as heavies

Fig. 9a shows the charge compensation as a function of rapidity along the jet axis for negative and positive fast particles separately, disregarding their identity. There is a strong short-range correlation, which is more pronounced for negative fast particles, and a much weaker long-range correlation, which also depends on the charge of the fast particle.

If we now require the associated particle to be a pion, the charge compensation has similar strength for both charges of the fast particle, as shown in fig. 9b. However, a clear difference in charge compensation is seen when the associated particle is a heavy particle (h) (fig. 9c).

In fig. 10 we require that both the fast particle and the associated particle should be identified as π or heavy. We notice the following effects: fast π^+ particles show much less short-range charge compensation

by h particles than do fast π^- particles; fast h^- particles have stronger

charge compensation by other h particles than do fast h^+ particles;

whereas the compensation of the charge of a heavy particle by pions is

equally strong for the two charges.

Short-range effects can be understood in a naïve model of quark frag-

mentation. First we discuss fast-π charge compensation by h particles, the

majority of which are kaons. A fast π^+ often contains a valence u quark

from the proton and a $\bar{d}$ quark from a $d\bar{d}$ pair creation. The remaining

d quark cannot form a K^-, thus suppressing a short-range compensation of

the leading π^+ by charged kaons. On the other hand, a fast π^- ($d\bar{u}$)

can get a K^+ ($u\bar{s}$) as a close partner, giving rise to a short-range effect.

Short-range effects from resonance production should be charge symmetric

for the π,K case.

A possible explanation for the charge compensation being stronger for

h^-h (most of them are leading K^-) than for h^+h (most of them are leading

K^+) is as follows. The K^+ ($u\bar{s}$) can be formed from a scattered valence

u quark from the proton. Certainly there must be an associated s quark,

but this s quark can materialize as a K^-, $\bar{K}^0$, or even as a strange baryon.

On the other hand, K^- ($\bar{u}s$) contains no valence quark in common with the

proton, and so we have both an associated u quark and an associated

$\bar{s}$ quark, strongly favouring the production of an associated K^+. However,

the whole effect could also be explained by a general surplus of protons

over antiprotons.

4.2 Fast heavy particles separated into kaons and protons

With more limited statistics we can separate the heavy particles into identified kaons and protons. For the associated particles, identification by drift chamber dE/dx extends only to momenta of ~1 GeV/c. There is therefore a large rapidity gap between the fast particles and identified kaons and protons, preventing a study of short-range effects in this case. In fig. 11 we show the charge compensation by pions, kaons, and protons for a pion, kaon, and proton fast particle. The kaon effect discussed in subsection 4.1 is compatible with the data but is not statistically significant.

We find that the charge compensation difference between positive and negative triggers for different species of associated particles comes mainly from a strong effect for associated protons. The effect is clearly established for fast pions and kaons, and shows no dependence on rapidity, which excludes a pure resonance effect (Δ^{++}). A simple interpretation is that there is a general surplus of protons compared with antiprotons uncorrelated with the trigger particle, as we will see below.

The Lund model predictions for these effects are shown as lines in figs. 9-11. We see that the model reproduces the main features of the data. Given the somewhat different composition of particles as seen in figs. 6 and 7, we cannot expect a detailed agreement for figs. 9 and 10.

5.   CORRELATIONS BETWEEN PROTONS AND ANTIPROTONS

5.1 Associated protons and antiprotons at low p_T

The inclusive proton and antiproton production at high p_T was found not to be very well reproduced by the Lund model (see Section 3).

The underlying assumption for baryon production through diquark-antidiquark string-breaking can be more directly tested by studying the correlations between protons and antiprotons. No such identified pairs are, however, available in the Cherenkov arm, but at lower momentum the dE/dx measurement in the drift chamber permits a large sample of protons and antiprotons to be identified. It is possible to define an interval in p_T where the $\bar{p}p$ acceptance is uniform in the centre of mass, $0.55 < p_T < 0.9$ GeV/c, and we can study how protons and antiprotons in this p_T range range are correlated to the trigger particle, which is required to have a p_T larger than 3 GeV/c. We will study the distribution in $\Delta\varphi$, the difference in azimuthal angle between the trigger particle and the associated particle. Tracks are lost in the 16° wedges up and down in the drift chamber, but we can correct for these losses since the distribution of the trigger tracks in azimuth is wider than the size of the holes. We also correct for a loss of associated tracks within 6° of the trigger particle due to a limited resolution for close tracks in the drift chamber.

In fig. 12a we show the acceptance-corrected distribution in $\Delta\varphi$ between an h^+ trigger and associated antiprotons and between a π^+ trigger and antiprotons. The $\Delta\varphi$ distribution is normalized by the number of triggers. The latter distribution gives the general charge correlation behaviour without any contribution from trigger protons. We find that most of the $h^+\bar{p}$ correlation exhibits the same behaviour except for a very small enhancement near the trigger particle ($\Delta\varphi \sim 0$). This weak effect is probably due to proton-antiproton pairs. Figure 12b shows the corresponding case for h^- triggers with associated protons and for π^- triggers with protons. The correlations of associated protons and antiprotons with the trigger particle are very similar.

The Lund model predictions are shown in fig. 12 as a full line for π trigger cases, and as a dashed line for antiprotons associated with an h^+ trigger (fig. 12a) and for protons associated with an h^- trigger (fig. 12b). We see that the antiproton-proton correlation in $\Delta\varphi$ is very weak in the data -- in fact it is hardly seen -- in contrast with the large effects anticipated in the Lund model. Even if we reduce the proton (antiproton) part of the $h^{+\ (-)}$ trigger in the model, as suggested from the results shown in fig. 7, it still predicts too strong correlations.

In table 2 we give the proton and antiproton production rate per trigger, corrected for acceptance losses, for the different triggers types. The protons/antiprotons are summed over the full range in φ, $0.55 < p_T < 0.9$ GeV/c, and $-0.44 < y < 0.44$. The errors shown are statistical only; the systematic errors between the different trigger types are negligible. The over-all acceptance for identified protons and antiprotons in this part of phase space has been estimated to be 76% (corrected for in the table 2) with a systematic error of 15%. This estimate was obtained from a comparison of the inclusive proton and antiproton spectra, measured in minimum bias data, with published cross-sections [13].

The p and $\bar{p}$ triggered data are a subsample of the h^+ and h^- triggered data and have a trigger particle with mean p_T of 5.5 GeV/c, whereas the π,h triggers have a mean p_T of 4.1 GeV/c.

Table 2 shows that the production of low-momentum (p $_T\sim$ 0.7 GeV/c) protons and antiprotons is roughly independent of the identity of the trigger particle, except for a small charge effect and a somewhat larger $p,\bar{p}$ correlation. The sizeable correlation in rate does not, however, give rise to any clear angular correlation, as discussed above. The Lund model gives too few associated protons and antiprotons except for the $\bar{p}$(trigger)p(associated) and p(trigger)$\bar{p}$(associated) cases.

5.2 Associated heavy particles at high p_T

In another paper [14], where we discuss a data sample taken with a calorimeter trigger selecting antiprotons with a mean p_T of ~1 GeV/c, we have reported a tendency for the baryon number to be conserved within the trigger hemisphere. The ratio of the associated p/π^+ on the same side as the trigger was found to be 0.213 $\pm$ 0.005, whereas on the away side it was only 0.141 $\pm$ 0.003. With the higher p_T of the trigger in the present sample, the same ratio, in the same apparatus, for the $\bar{p}$ (h^-) trigger particle is only 0.114 $\pm$ 0.034 (0.116 $\pm$ 0.008) on the same side, which is even smaller than the value 0.146 $\pm$ 0.031 (0.143 $\pm$ 0.008) found for the away side. We find that this ratio depends neither on the p_T of the trigger particle within the range 3-8 GeV/c, nor on the p_T of the associated protons, which is however limited to 0.55 < p_T < 0.9 GeV/c.

One essential difference between the data of ref. 14 and the present sample is the proximity of the proton and antiproton in momentum space. The minimum Δp_T so far investigated here is 2 GeV/c. In order to minimize Δp_T but still use the trigger p or $\bar{p}$ as one of the pair, we shall use the high-pressure Cherenkov (HPC) to identify associated K,p (heavy) particles. The threshold of the HPC for π/h separation is at p_{lab} = 1.5 GeV/c. It is required that the associated particle be separated from the trigger particle in azimuthal angle by 6° < $|\Delta\varphi|$ < 30° in order to get equal acceptance for different combinations of charges. Within this $\Delta\varphi$ region, we define $R_{opp/same}$ as the ratio of the number of associated particles with charge opposite to the trigger, to the number with the same charge. In table 3 we see that the value of $R_{opp/same}$ is much larger for associated h particles than for associated π particles. Table 4 shows the ratios in the same $\Delta\varphi$ region for associated particles identified in the drift

chamber. As already explained, Δp_T is now at least 2 GeV/c, and one sees much reduced h^+h^- and h^-h^+ correlations.

Thus there is indeed a strong compensation of charge between h particles provided they are sufficently close in phase space. The numbers in parentheses are predictions of the Lund model incorporating the constraints of the experiment. The data of table 3 are reasonably well described by the model, but the predicted hh correlation as the particles become more separated, is too strong (see table 4).

It is interesting to note the local charge correlation between the h particle and accompanying fast pions (see table 3). It is somewhat stronger than predicted by the model, suggesting a possible mechanism of diquark splitting in which a meson, rather than an antibaryon, is produced in the break up of the colour field [15]. Such a mechanism would also weaken the angular correlation between associated protons (antiprotons) and $h^{-\,(+)}$ trigger particles, as observed in our data. It is further supported by the h^+/π^+ ratio of HPC-identified associated particles for an h^- trigger, which is found to be 0.26 ± 0.06, whereas the Lund model gives the very high value of 1.25 ± 0.07. (In order to get the same acceptance for the h^-h and $h^-\pi$ combinations, only tracks traversing different modules in the HPC, and thus separated by $20° < |\Delta\varphi| < 30°$ have been used.)

The local compensation of baryon number in e^+e^- annihilations has recently been reported by the TASSO Collaboration [16] to be in agreement with the Lund model.

6.   **AWAY-SIDE CORRELATIONS**

The compensation of trigger charge was seen to extend into the away side (long-range effects, fig. 9). Usually the away-side jet is balanced

in azimuth (p_T plane) in an event with a high-p_T trigger particle, whilst the polar angle varies from event to event. Thus to study the away side we choose a variable depending on the p_T of the associated particles, instead of the rapidity along the trigger-jet axis. This is the usual x_E variable:

$$x_E = -\vec{p}_T(ass) \cdot \vec{p}_T(trig) / [p_T(trig) \cdot p_T(trig)] \ .$$

A particle is said to belong to the away side if $x_E > 0$.

The charge ratio, $R^{+/-}$, of the mean densities of positive and negative particles is studied as a function of x_E in subsection 6.1 for unidentified particles, and in subsection 6.2 for identified particles.

Correlations between a high-p_T trigger and charged particles on the away side have been studied by, for example, the BFS Collaboration [3] at essentially the same c.m. energy, using the SFM detector.

6.1 Unidentified associated particles

Figure 13a shows the charge ratio $R^{+/-}$ on the away side versus x_E for positive and negative pion triggers. The charge ratio grows with x_E and is similar for both trigger charges but with an over-all larger positive excess for negative triggers. Just as was found in the case of charge compensation versus rapidity, we find the low-x_E particles to be influenced by the trigger charge. The clear rise of $R^{+/-}$ with increasing x_E is in agreement with the assumption that the leading away-side particle more often contains a scattered u valence quark than a d quark.

Our previously published π^0 triggered data [17] fall roughly in the middle between our positive and negative trigger data, confirming the influence of the trigger charge on the away side, at least at low x_E. At high x_E the values of $R^{+/-}$ for π^+, π^-, and π^0 triggered data are very

similar, supporting the simple idea that scattered charged partons are predominantly valence u quarks.

The Lund model gives smaller values of $R^{+/-}$ for the higher values of x_E, as shown by the hatched area in fig. 13. Figure 13b shows the charge ratio on the away side versus x_E for positive and negative heavy triggers. The BFS Collaboration has reported a higher ratio opposite an h^- trigger [3]. They studied density ratios of away-side particles with a p_T of more than 1.5 GeV/c, and found a 3σ difference in the charge structure opposite an h^- trigger compared to that opposite π and h^+ triggers. The results of our measurements are compatible with theirs but do not show any significant effect. A detailed comparison has been made elsewhere [18].

6.2 Identified associated particles

Particle identification using dE/dx in the central detector separates pions, kaons, and protons at low momentum. In table 5 we give the charged ratios $R^{+/-}$ integrated over the small x_E range of identification, $0 < x_E < 0.3$, together with corresponding results from the Lund model.

For away-side kaons the ratio $R^{+/-}$ for h^- triggers is larger than for π^- triggers (a 3σ effect), whilst for π^+ and h^+ triggers these ratios are roughly equal. To interpret this effect we consider the h^- as being a K^-. If the correlation were due to the decay of a particle $X \rightarrow K^+ K^-$, it should be present for h^+ triggers as well. An invariant mass plot contains no significant signal. We thus interpret this effect in the same way as in subsection 4.1, which in this case means that the fragmentation giving rise to a leading K^- on the trigger side will in some cases produce a correlated K^+ on the away side.

The largest $R^{+/-}$ values are found for away-side protons, in line with Section 5.

The Lund model reproduces essentially the features as seen in data at low x_E, and its predictions are also given in table 5.

7. CONCLUSIONS

The composition of the charged particle flux around $\theta = 90°$ in the c.m.s. has been measured in pp collisions at the energy $\sqrt{s} = 63$ GeV for transverse momenta up to 8 GeV/c.

For the charge correlations between an identified high-p_T particle and associated particles we find that the charge compensation on the same side as the trigger depends strongly on the identity of the associated particles and on the identity of the trigger particle. The compensation follows qualitatively a simple picture of quark fragmentation, and the effects are generally reproduced by the Lund model of pp collisions. However, this model has difficulties in describing baryon effects, and the data suggest a more elaborate mechanism for baryon production.

Particle production on the away side is influenced by the trigger charge. The +/- ratio of low-p_T away-side particles is significantly larger for negative triggers than for positive triggers. The ratio grows with x_E, as expected for flavour-independent parton scattering.

REFERENCES

[1] B. Alper et al. (BS Collab.), Nucl. Phys. B100 (1975) 237.

[2] A. Breakstone et al. (ABCDHW Collab.), Phys. Lett. 135B (1984) 510.

D. Drijard et al. (CDHW Collab.), Nucl. Phys. B208 (1982) 1.

[3] M.G. Albrow et al., Nucl. Phys. B145 (1978) 305.

[4] D. Drijard et al. (CDHW Collab.), Nucl. Phys. B166 (1980) 233.

D. Drijard (CDHW Collab.), preprint CERN-EP/82-212 (1982), presented

at the Europhysics Study Conf., Erice, 1982.

W.M. Geist (CDHW Collab.), Proc. Summer Institute on Particle

Physics, Stanford, 1982 (SLAC report 259, Stanford, 1983),

p. 389.

[5] H.-U. Bengtsson, Lund preprint LU-TP 82-15 (1982), and references

given therein, to appear in Comput. Phys. Commun.

The simulation presented was made using a primordial k_T with a

Gaussian width of 0.85 GeV/c and a cut-off at 1.7 GeV/c. Setting

the primordial k_T to zero does not change significantly any of the

results presented in this paper.

[6] H. Gordon et al., Nucl. Instrum. Methods 196 (1982) 303.

O. Botner et al., Nucl. Instrum. Methods 196 (1982) 315.

[7] B. Heck et al., preprint CERN-EF/80-05 (1980).

S. Cairanti et al., Proc. Topical Conf. on the Application of Micro-

processors to High-Energy Physics Experiments, Geneva, 1981

(CERN 81-07, 1981), p. 321.

[8] S. Almehed and B. Lörstad, Comput. Phys. Commun. 22 (1981) 209.

[9] B. Andersson, G. Gustafsson and T. Sjöstrand, Nucl. Phys. B197 (1982)

45.

[10] R. Brandelik et al., Phys. Lett. $\underline{100B}$ (1981) 357.

[11] C. Berger et al., DESY 82-058 (1982).

[12] T. Sjöstrand, Comput. Phys. Commun. $\underline{28}$ (1983) 229.

The jet algorithm was used with a small value (1.0 GeV/c) of the principal parameter, d_{join}, to determine the jet directions with negligible influence from particles outside the jet.

[13] U. Mjörnmark, Thesis, University of Lund (1983).

[14] T. Akesson et al., preprint CERN-EP/84-26, submitted to Nuclear Physics B.

[15] A. Bartl et al., Phys. Lett. $\underline{122B}$ (1983) 427.

The Lund model is developing along these lines at the moment (private communication, G. Gustafsson).

[16] M. Althoff et al., DESY 84-004 (1984).

[17] T. Åkesson et al., Phys. Lett. $\underline{118B}$ (1982) 178.

[18] A. Nilsson, Thesis, University of Lund (1983).

Table 1

The +/- ratio and the relative frequency of the trigger particles as a function of p_T. The errors are statistical only.

a) The +/- ratio of the trigger particles

$\langle p_T \rangle$	$R^{+/-}$
GeV/c	
4.09	1.18 ± 0.02
4.52	1.20 ± 0.03
4.96	1.27 ± 0.04
5.39	1.28 ± 0.06
5.83	1.25 ± 0.08
6.44	1.32 ± 0.09
7.31	1.60 ± 0.19
8.18	1.58 ± 0.31
9.48	1.60 ± 0.43

b) The ratio π/all

$\langle p_T \rangle$	Positives	Negatives
GeV/c		
2.79	0.567 ± 0.011	0.656 ± 0.011
3.27	0.591 ± 0.008	0.691 ± 0.008
3.75	0.610 ± 0.007	0.716 ± 0.007
4.22	0.630 ± 0.010	0.734 ± 0.009

c) The relative frequency of π, K, and p

$\langle p_T \rangle$	π^+	π^-	K^+	K^-
GeV/c				
5.4	0.359 ± 0.011	0.321 ± 0.009	0.136 ± 0.011	0.074 ± 0.008
6.4	0.366 ± 0.014	0.318 ± 0.010	0.141 ± 0.011	0.070 ± 0.008
7.4	0.371 ± 0.027	0.290 ± 0.019	0.155 ± 0.011	0.096 ± 0.018

$\langle p_T \rangle$	p	$\bar{p}$
GeV/c		
5.4	0.075 ± 0.009	0.045 ± 0.006
6.4	0.069 ± 0.009	0.036 ± 0.006
7.4	0.066 ± 0.017	0.021 ± 0.009

Table 2

The number of associated protons and antiprotons per trigger

a) Number of associated protons per trigger

Trigger	Data	Lund model
π^+	0.066 ± 0.003	0.027 ± 0.001
π^-	0.070 ± 0.003	0.033 ± 0.001
h^+	0.067 ± 0.003	0.027 ± 0.001
h^-	0.086 ± 0.004	0.058 ± 0.002
p	0.055 ± 0.011	0.029 ± 0.005
$\bar{p}$	0.089 ± 0.017	0.085 ± 0.005

b) Number of associated antiprotons per trigger

Trigger	Data	Lund model
π^+	0.049 ± 0.003	0.023 ± 0.001
π^-	0.043 ± 0.003	0.023 ± 0.001
h^+	0.061 ± 0.003	0.046 ± 0.002
h^-	0.046 ± 0.003	0.022 ± 0.001
p	0.068 ± 0.016	0.062 ± 0.008
$\bar{p}$	0.047 ± 0.009	0.015 ± 0.005

Table 3

$R_{opp/same}$ for associated particles (p_T > 1.3 GeV/c)
identified in the HPC

Numbers in paranthesis are the predictions of the Lund model

Trigger particle	Associated particles	
	h	π
h⁻	6.3 ± 1.0 (7.0 ± 0.7)	2.3 ± 0.4 (1.7 ± 0.1)
h⁺	3.3 ± 0.4 (3.3 ± 0.2)	2.1 ± 0.3 (1.7 ± 0.1)

Table 4

$R_{opp/same}$ for associated particles (p_T < 1.3 GeV/c)
identified in the drift chamber

Numbers in paranthesis are the predictions of the Lund model

Trigger particle	Associated particles	
	h	π
h⁻	2.0 ± 0.2 (4.4 ± 0.7)	1.40 ± 0.07 (1.55 ± 0.03)
h⁺	1.2 ± 0.1 (2.7 ± 0.2)	1.27 ± 0.03 (1.31 ± 0.03)

Table 5

$R^{+/-}$ for identified associated particles
on the away side for different triggers

	Trigger	Identified associated particles		
		π	K	P
Data	π^+	1.09 ± 0.01	1.00 ± 0.04	1.53 ± 0.06
	h^-	1.04 ± 0.02	1.27 ± 0.08	1.58 ± 0.10
	π^+	0.95 ± 0.01	0.95 ± 0.04	1.33 ± 0.06
	h^+	0.95 ± 0.01	0.84 ± 0.05	1.16 ± 0.06
Lund model	π^-	1.07 ± 0.01	1.13 ± 0.05	1.31 ± 0.07
	h^-	1.06 ± 0.01	1.44 ± 0.10	1.73 ± 0.15
	π^+	0.99 ± 0.01	1.10 ± 0.05	1.20 ± 0.06
	h^+	1.02 ± 0.01	0.91 ± 0.05	1.08 ± 0.04

Figure captions

Fig. 1 : The Axial Field Spectrometer viewed transversely to the collision axis. The magnetic field is perpendicular to the plane of the paper.

Fig. 2 : The efficiency of the aerogel counter for pions. The pions below p_{lab} = 0.5 GeV/c are identified by dE/dx measurements in the drift chamber, and pions above p_{lab} = 1.5 GeV/c by the HPC.

Fig. 3 : The HPC performance showing the number of photoelectrons as a function of particle momentum. The band of pions is clearly separated from heavier hadrons.

Fig. 4 : The APC performance showing the number of events as a function of the number of photoelectrons for particles identified as non-pions by the HPC. The kaons and protons are well separated.

Fig. 5 : The fractional composition of the particle flux into pions, kaons, and protons, as a function of p_T , for a) positively charged particles; b) negatively charged particles.

Fig. 6 : The charge ratio $R^{+/-}$ of trigger particles as a function of p_T. The hatched area is the result of a simulation with the Lund model.

Fig. 7 : The fraction of different charged trigger particles as a function of p_T. The hatched areas are given by the Lund model.

Fig. 8 : The density of charged tracks, uncorrected for acceptance, as a function of the rapidity along the jet axis. The jet includes the trigger particle.

Fig. 9 : Charge compensation, $\tilde{A}(y)$ of particles in the interval

2 < y' < 5 (fast particles) as a function of rapidity along

the jet axis. The indices "f" and "ass" stand for fast particle

and associated particle, respectively:

a) all_f, all_{ass}: charge compensation of all fast particles by

all associated particles, regardless of their identifi-

cation;

b) all_f, π_{ass}: charge compensation of all fast particles by

associated particles identified as pions;

c) all_f, h_{ass}: charge compensation of all fast particles by

associated particles identified as heavier than pions.

The full line represents the Lund model calculation for

negative fast particles, the dashed line for positive fast

particles.

Fig. 10 : Charge compensation, $\tilde{A}(y)$, of identified fast particles (π or

h) in the interval 2 < y' < 5 by identified associated par-

ticles (π or h) as a function of rapidity y. Notation as in

fig. 9.

Full line represents the Lund model calculation for negative

fast particles, the dashed line for positive fast particles.

Fig. 11 : Charge compensation, $\tilde{A}(y)$, of identified fast particles (π, K

or p) in the interval 2 < y' < 5 by identified associated par-

ticles (π, K or p) as a function of rapidity y. Notation as in

fig. 9.

Full line represents the Lund model calculation for negative

fast particles, the dashed line for positive fast particles.

Fig. 12 : Distribution of the difference in azimuthal angle $\Delta\varphi$ between

a proton/antiproton, $0.55 < p_T < 0.9$ GeV/c, and the trigger

particle, $p_T > 3.0$ GeV/c.

a) The $\Delta\varphi$ distribution for antiprotons with respect to h^+

(crosses) and π^+ triggers (histogram). The full line repre-

sents the Lund model result for π^+ triggers, the dashed

line for h^+ triggers.

b) The $\Delta\varphi$ distribution for protons with respect to h^- triggers

(crosses) and π^- triggers (histogram).

The full line represents the Lund model result for π^- triggers,

the dashed line for h^- triggers.

Fig. 13 : Unidentified away-side particles. Charge ratio $R^{+/-}$ versus x_E

for different triggers:

a) π^- (empty circle) and π^+ (full circle) triggers;

b) h^- (empty square) and h^+ (full square) triggers.

The triggers are required to have $p_T > 3.0$ GeV/c.

The hatched areas and the lines represent the Lund model

results. The full line gives the charge ratio for negative

triggers, the dashed line that for positive triggers. At low

x_E a difference in charge ratio is seen, which depends on the

trigger charge.

COPPER CALORIMETERS

A.P CHERENKOV 1 atm.

1 m

CENTRAL HODOSCOPE

AEROGEL CHERENKOV

PROPORT. CH

H.P. CHERENKOV 4 atm.

VACUUM CHAMBER

DRIFT CHAMBERS

MAGNET COIL

MAGNET YOKE

Fig. 1

Fig. 2

Pulseheight in HPC

Photoelectrons

p_{lab} (GeV/c)
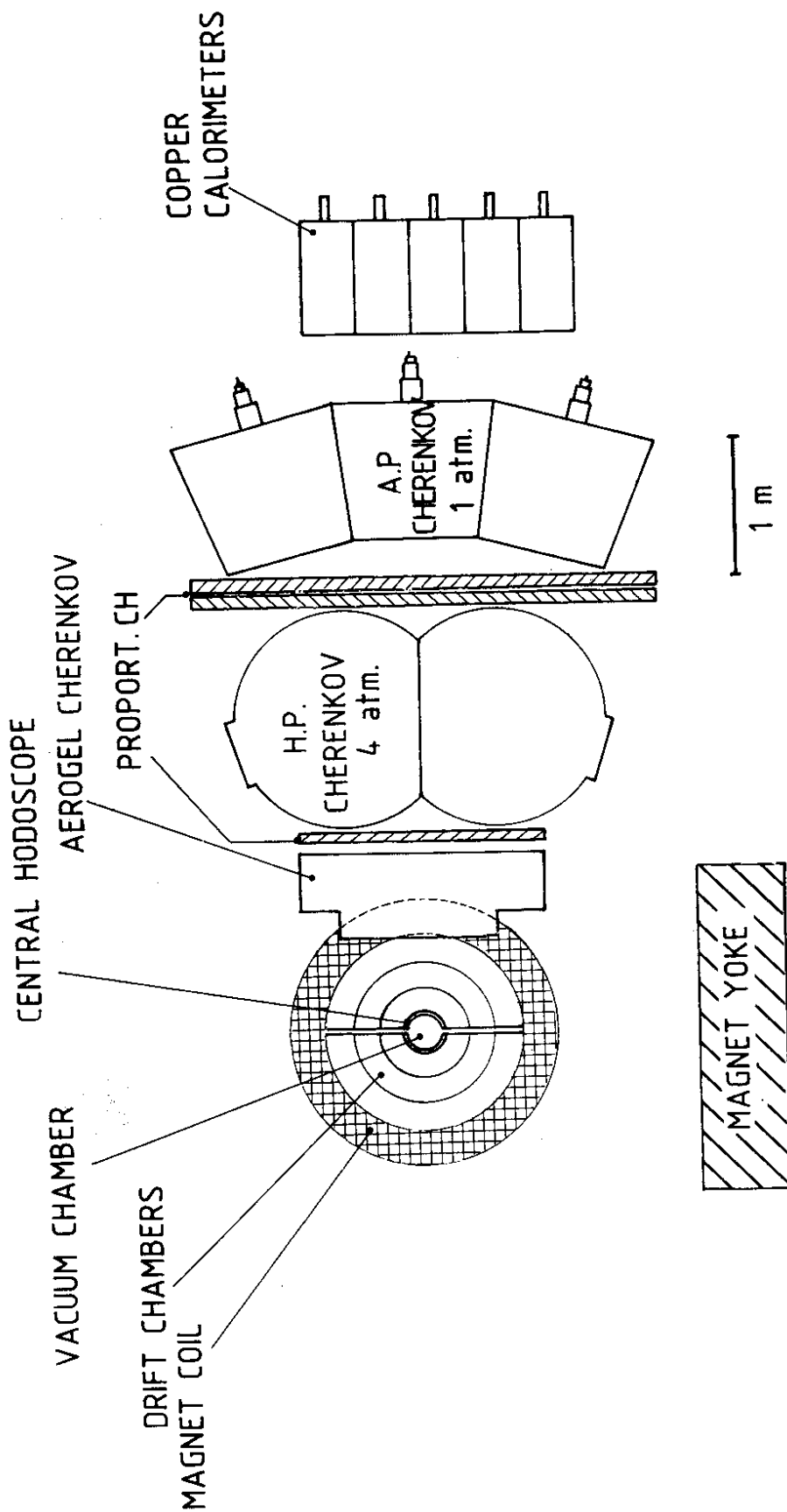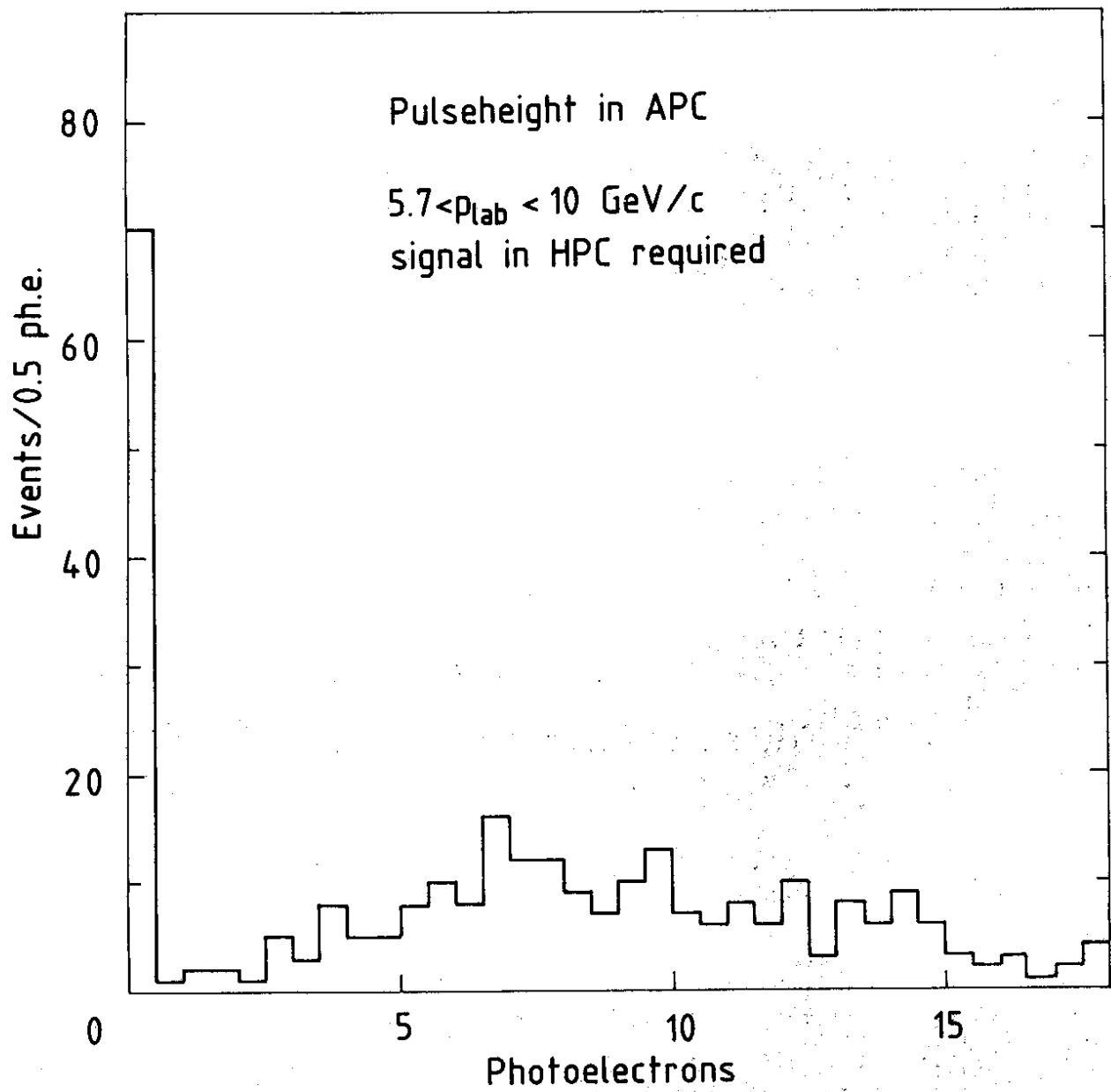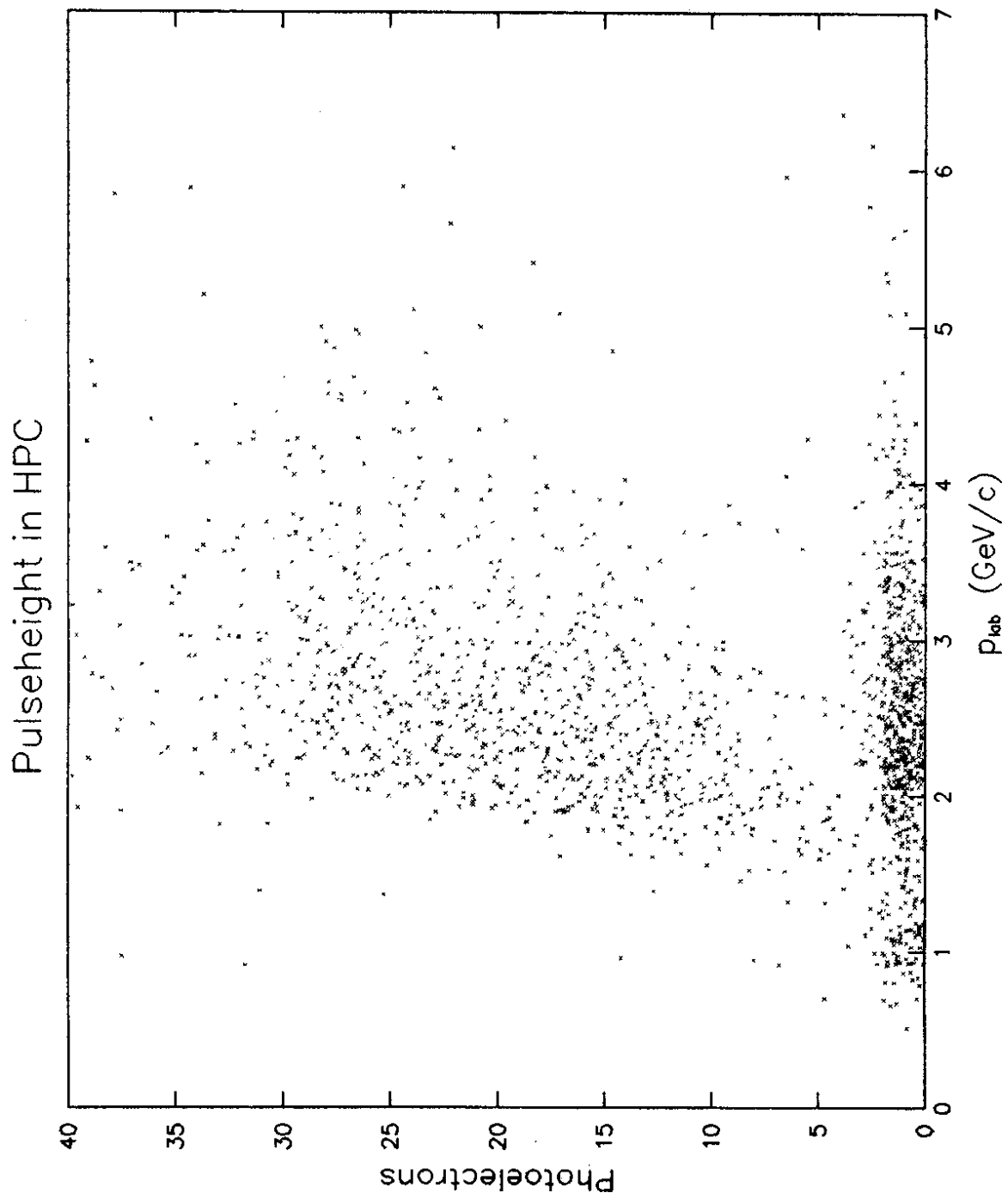
Fig. 3
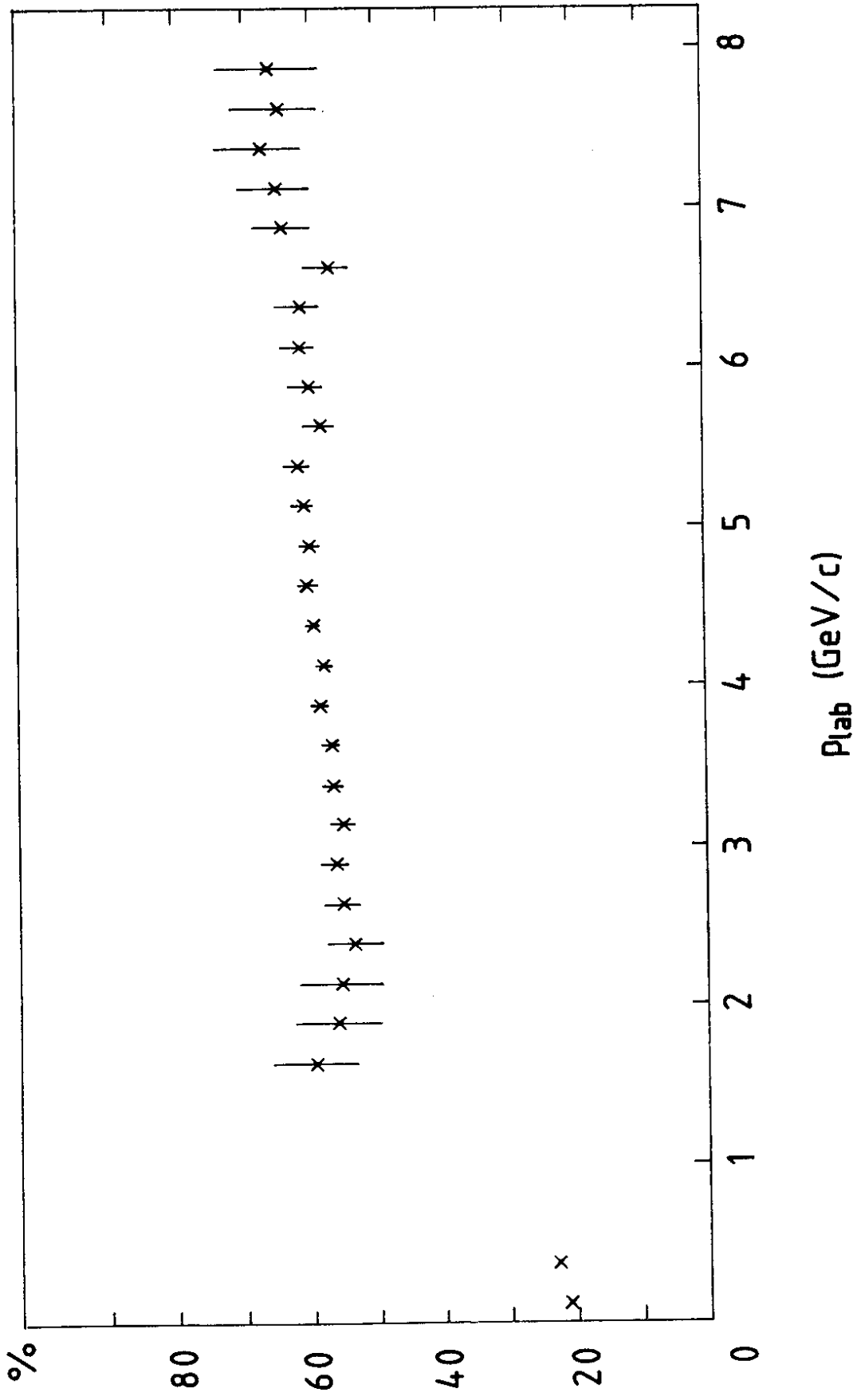
Fig. 4

PARTICLE COMPOSITON - POSITIVELY CHARGED PARTICLES

- ● This exp.
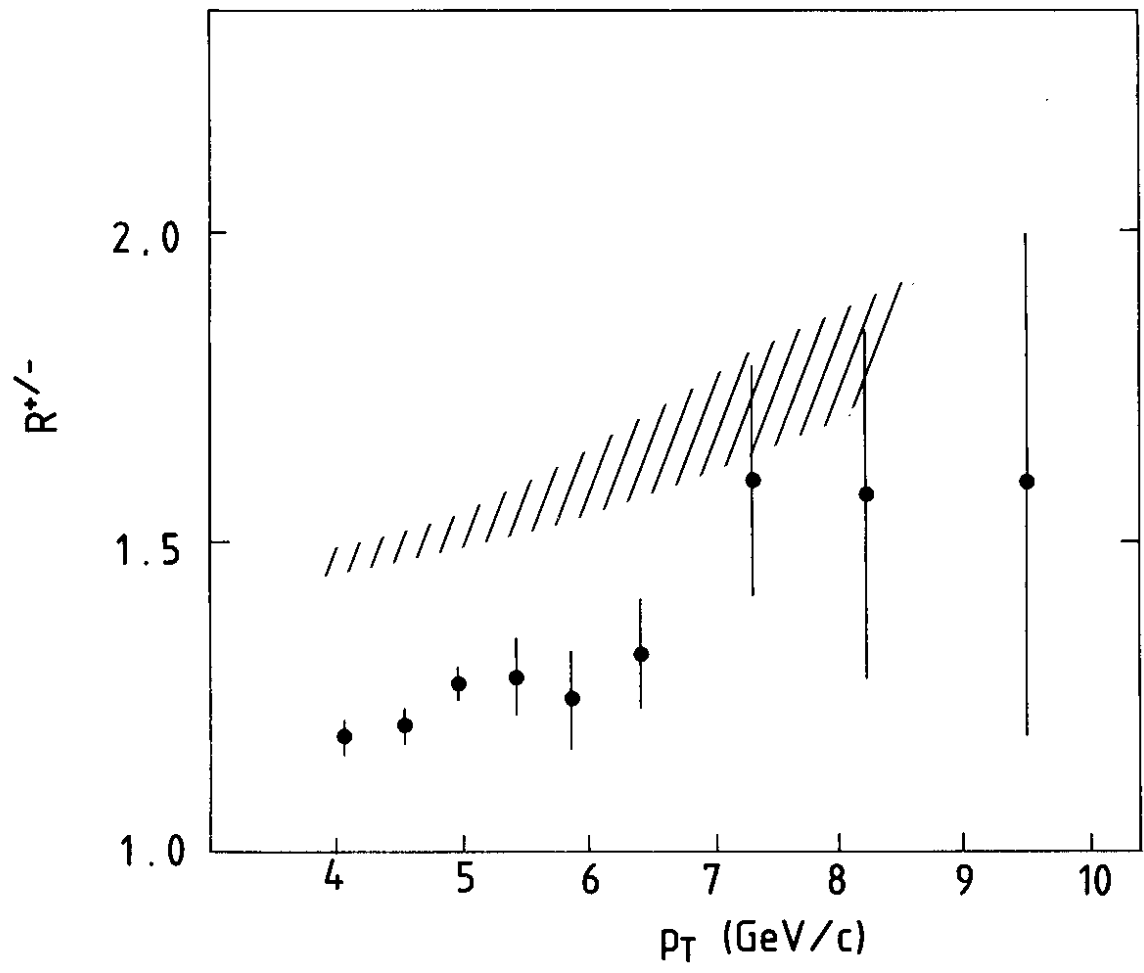- △ CDHW,⟨θ⟩=49°
- ---- Extrapolated from BS
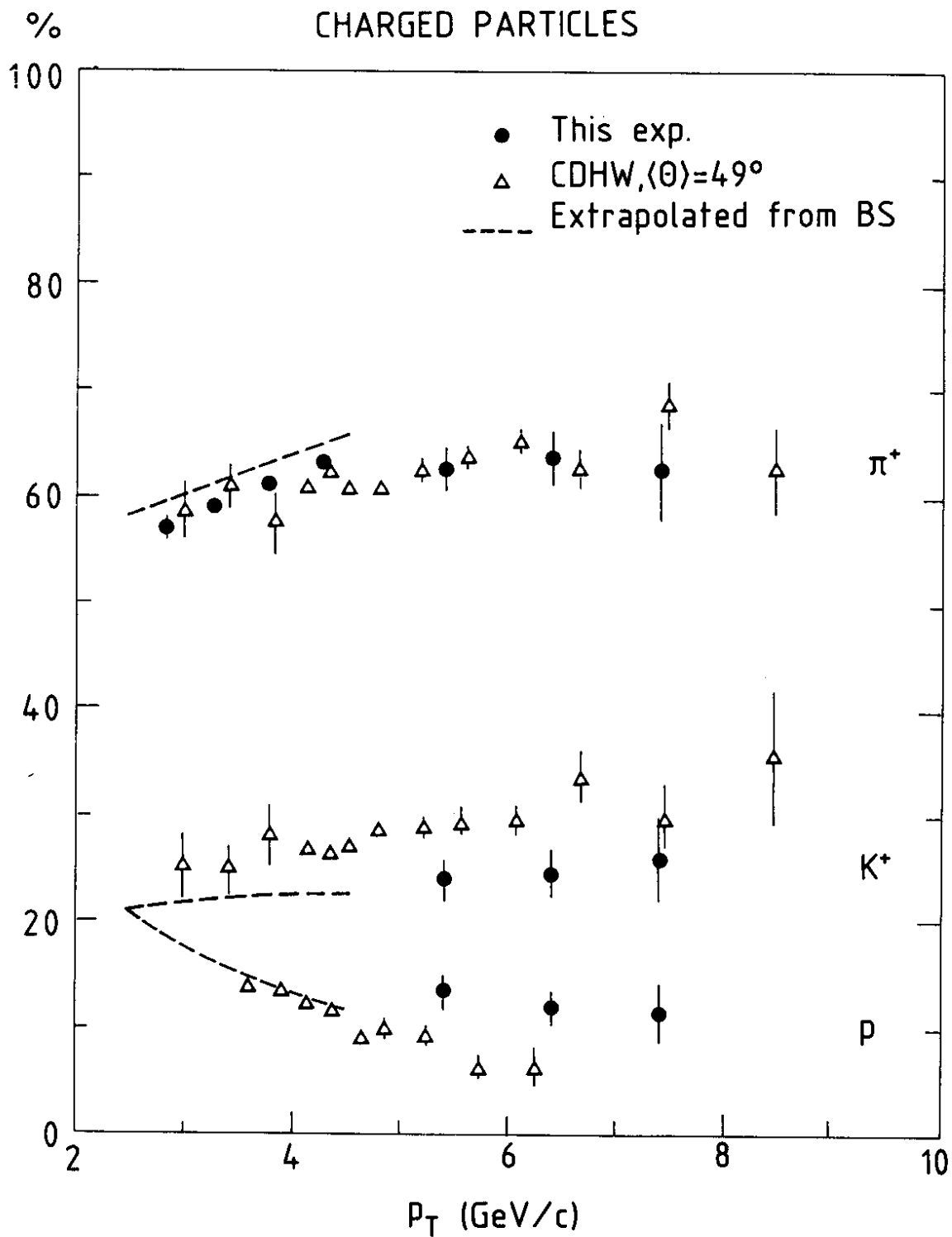
Fig. 5a
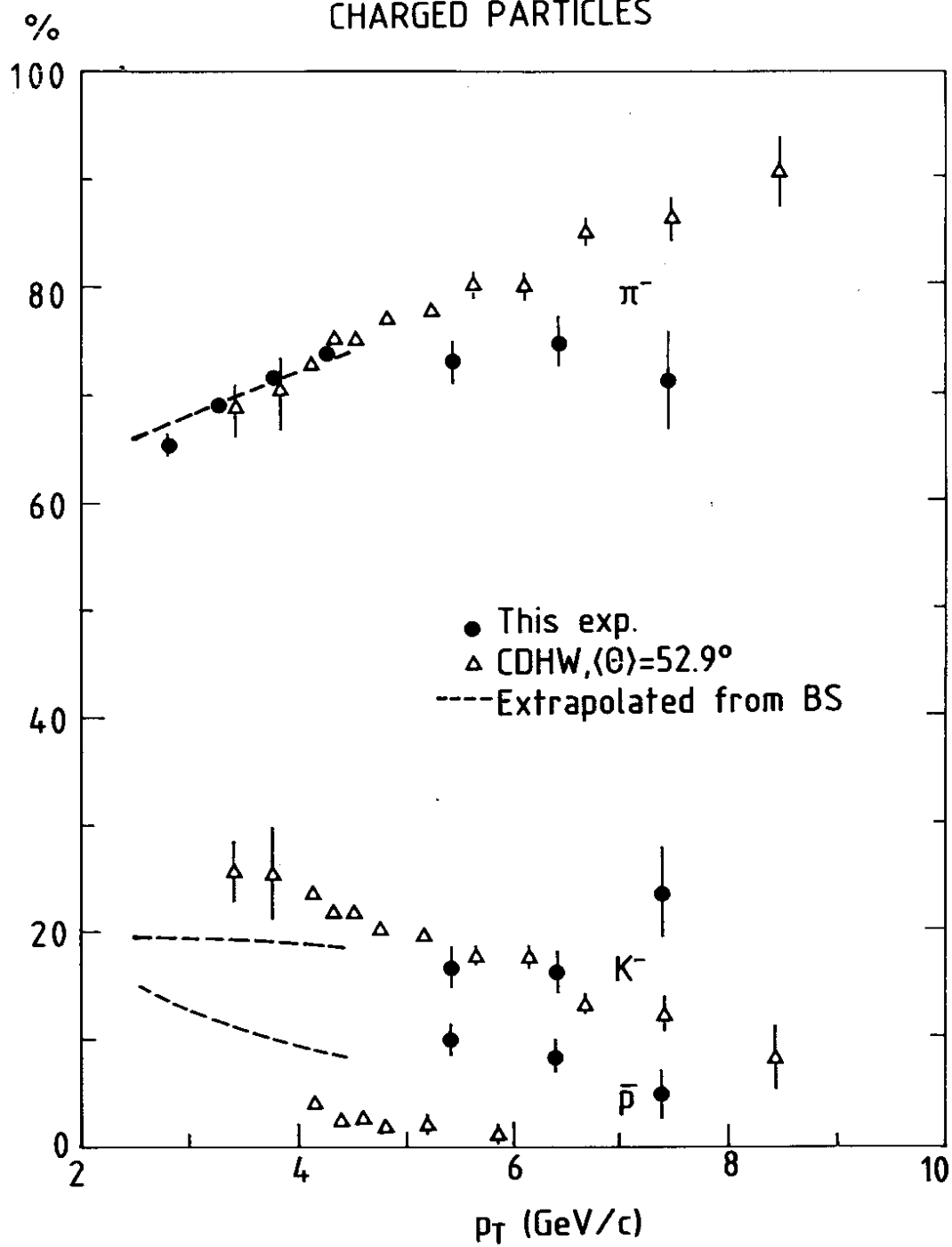
Fig. 5b
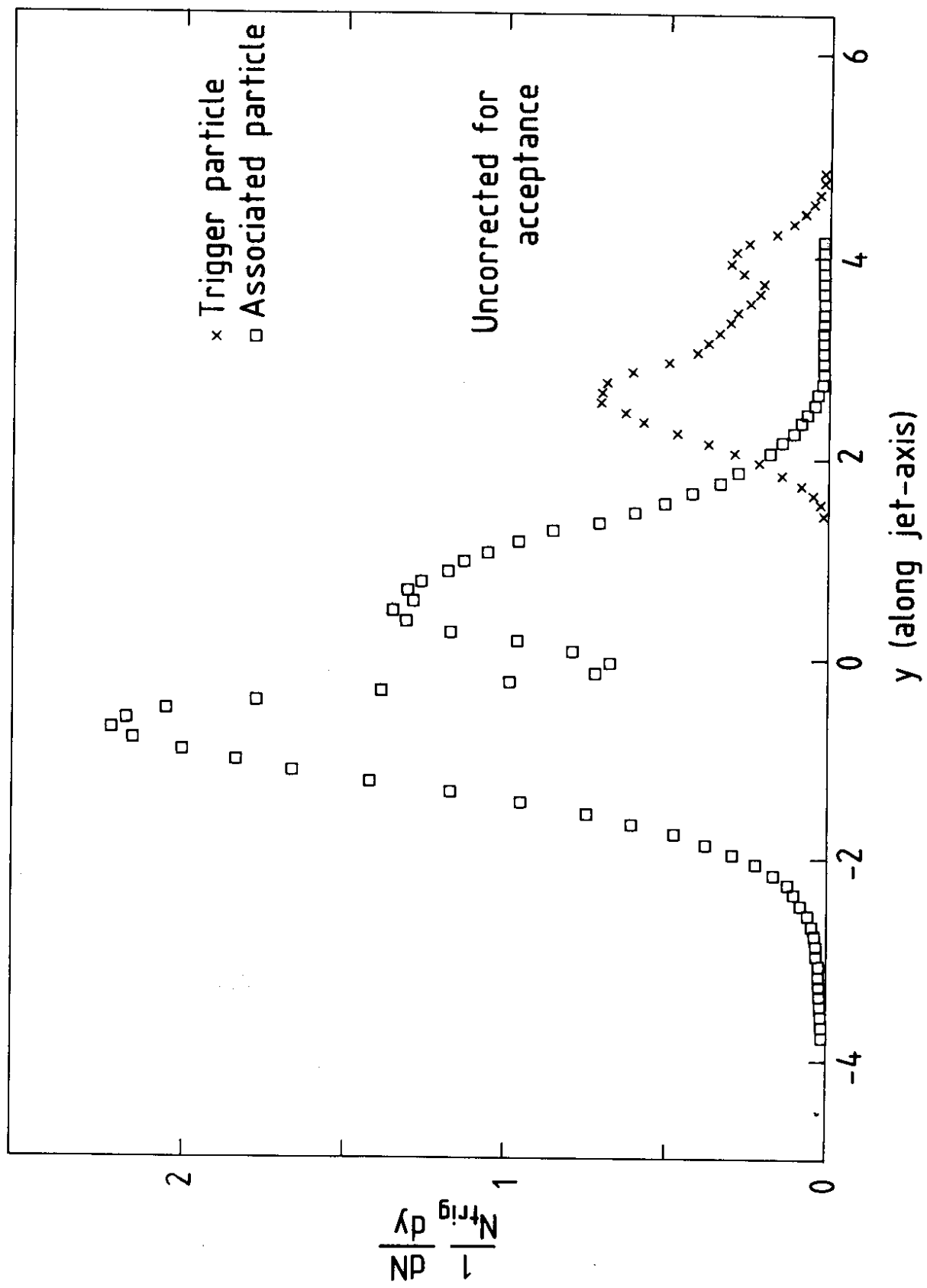
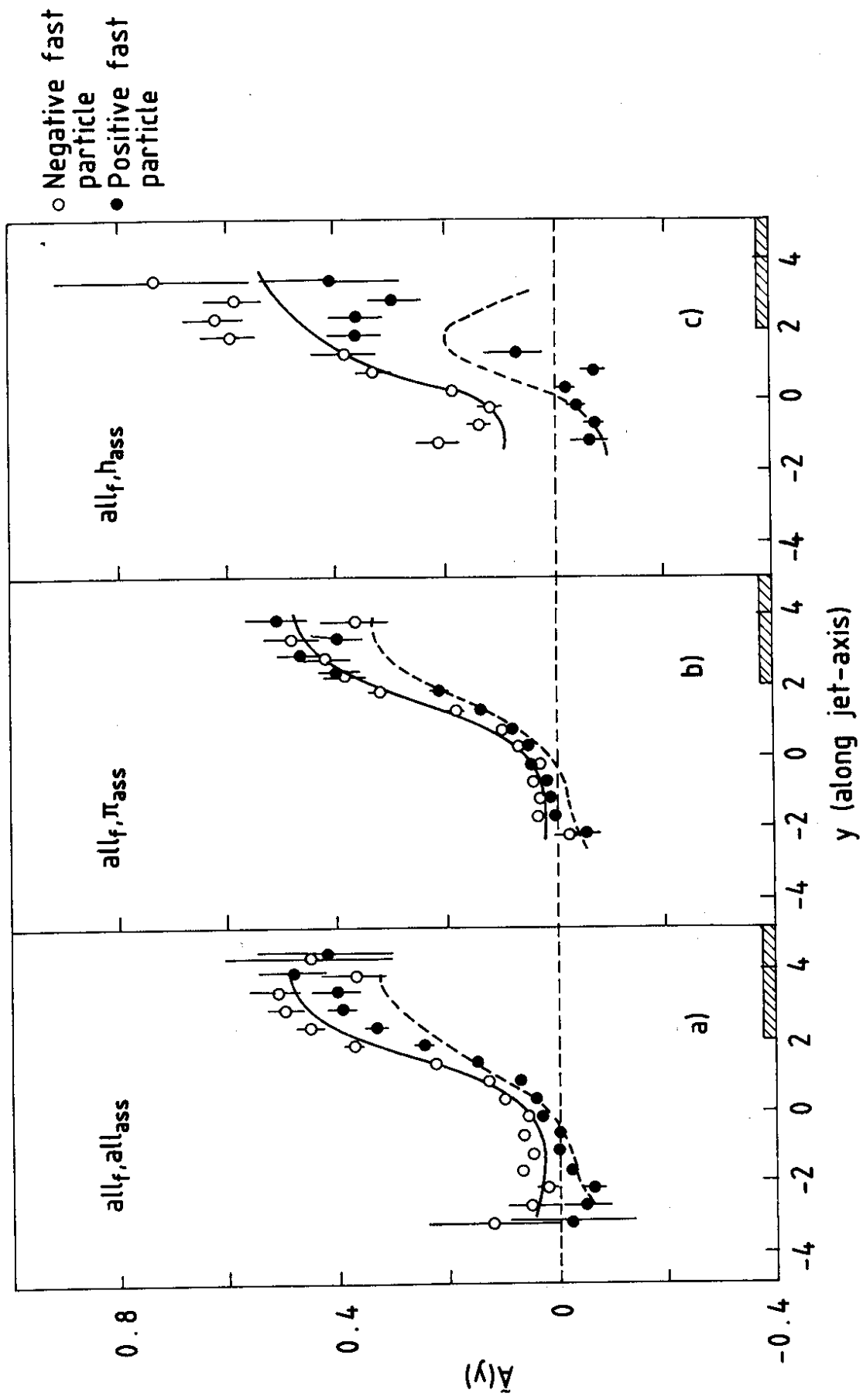Fig. 6

PARTICLE COMPOSITION –
ALL CHARGED PARTICLES

Fig. 7

× Trigger particle
□ Associated particle

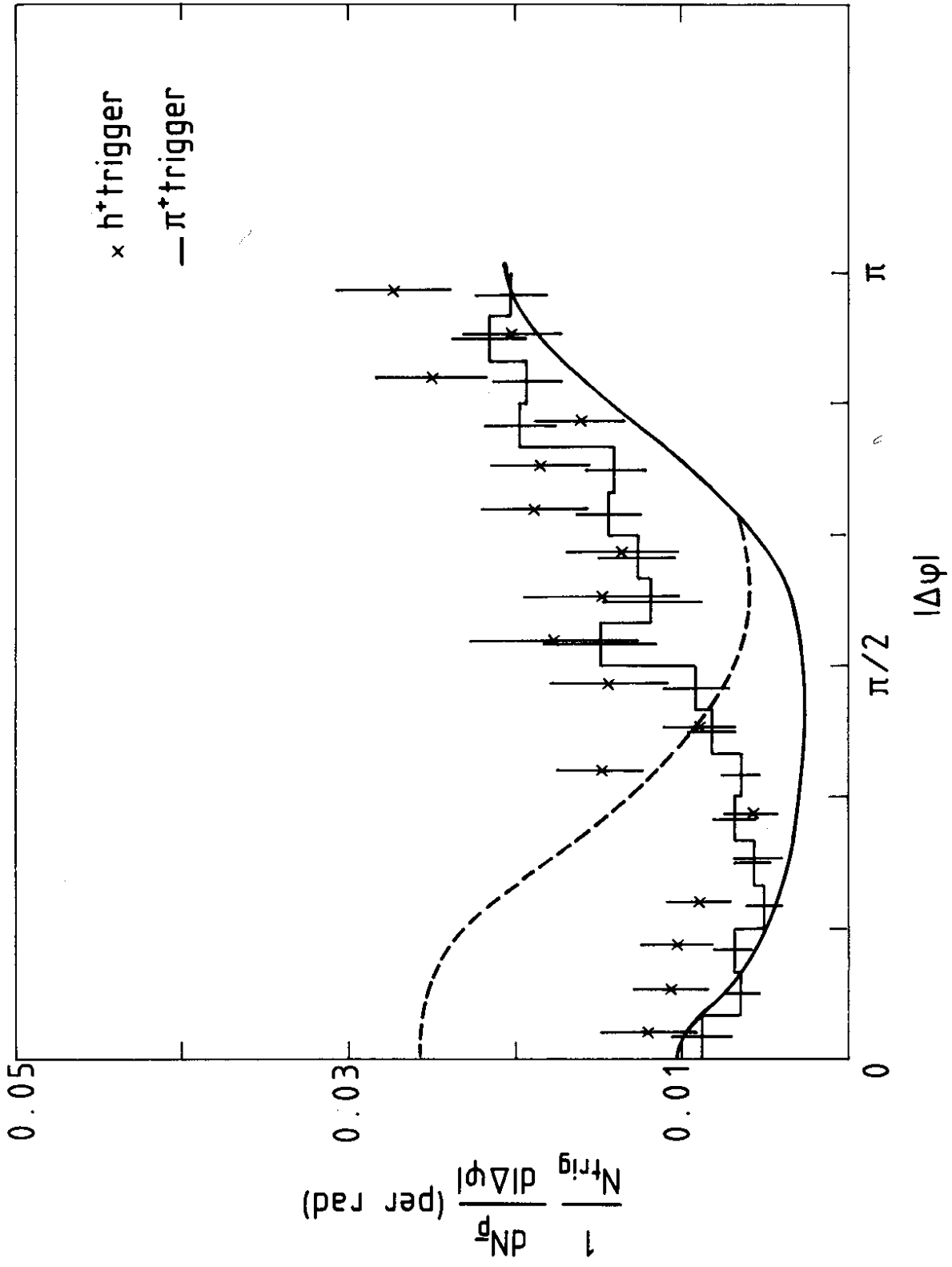Uncorrected for
acceptance

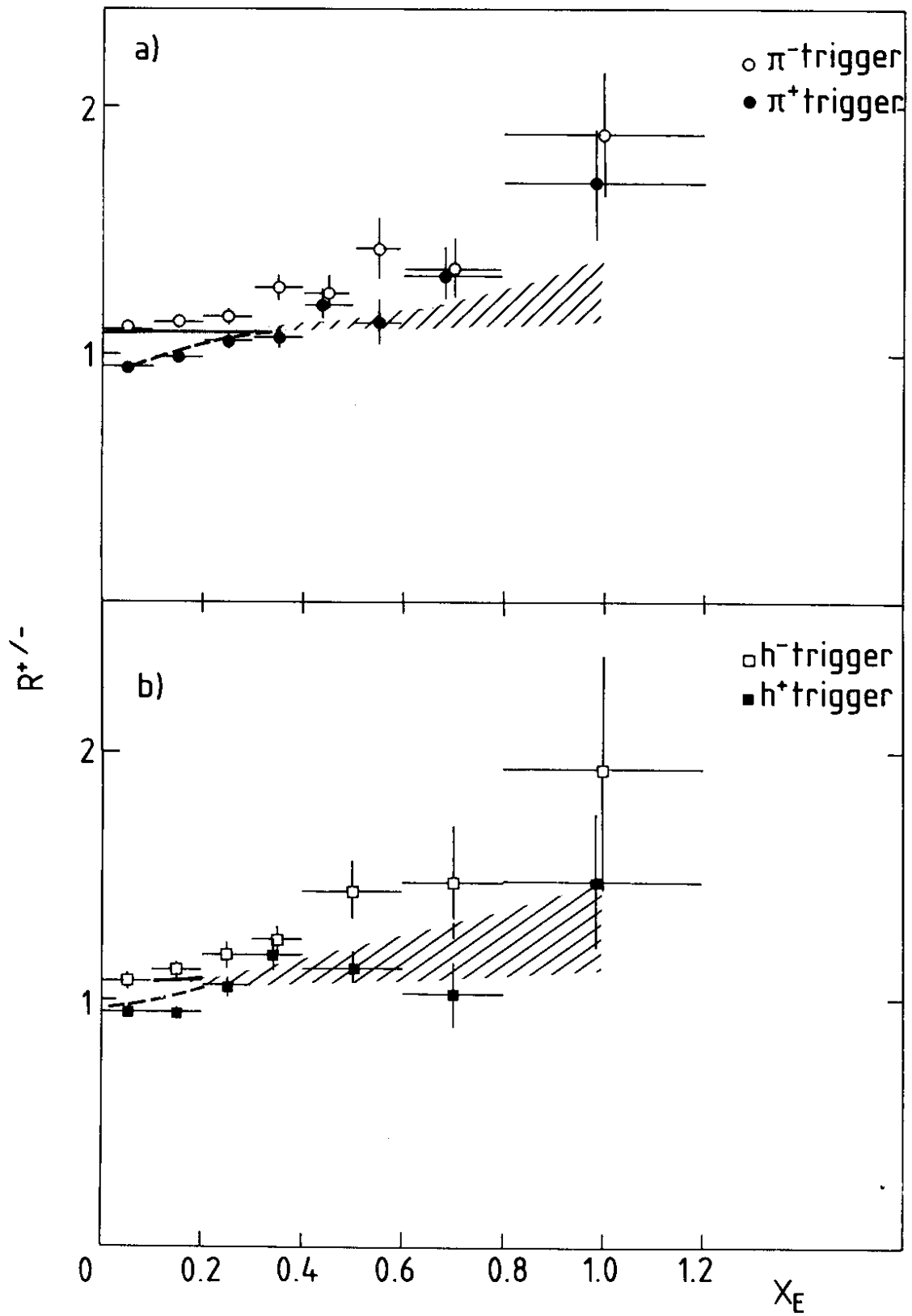$\frac{1}{N_{trig}}\frac{dN}{dy}$

y (along jet-axis)
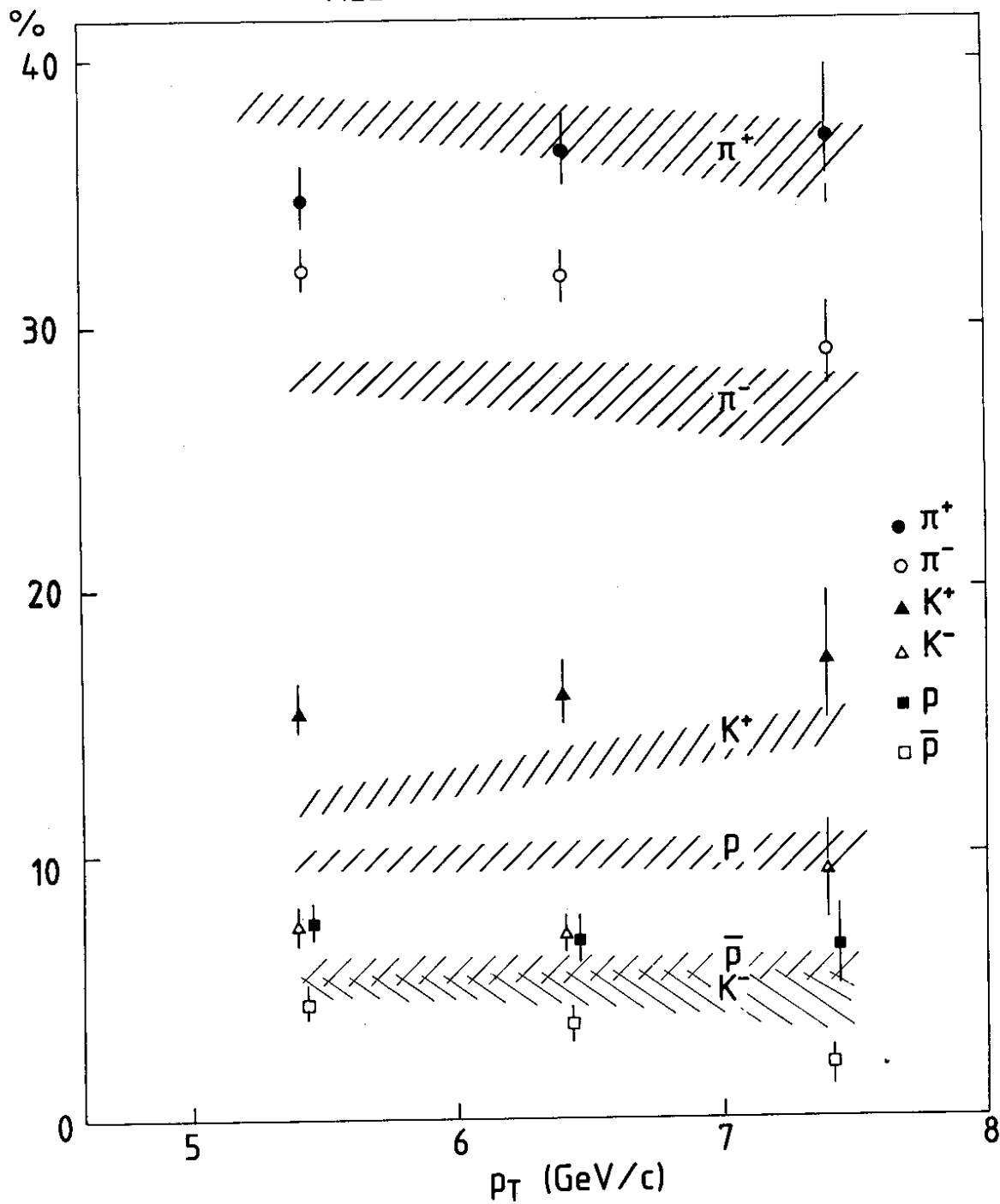
Fig. 8

Fig. 9
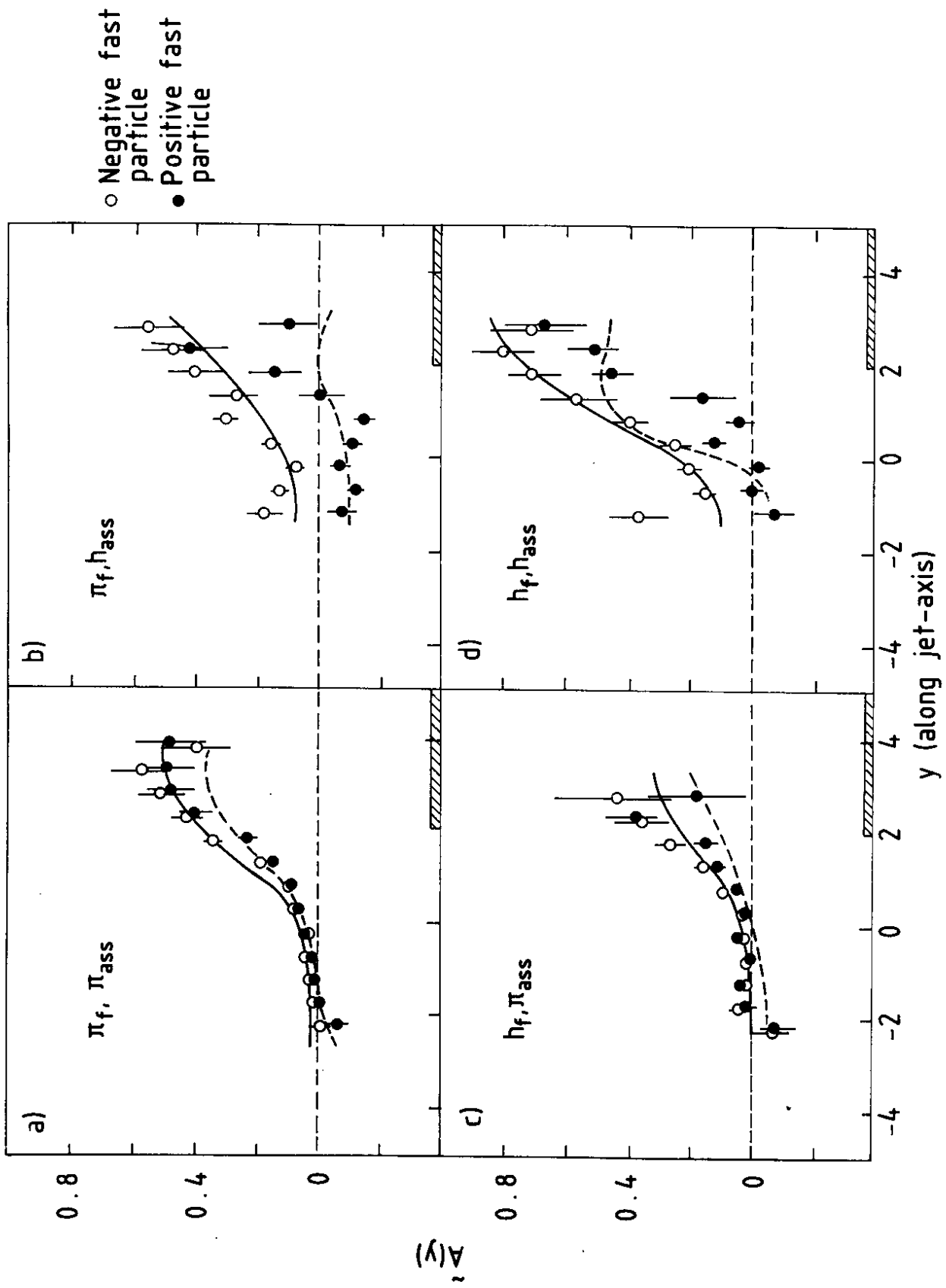
Fig. 10
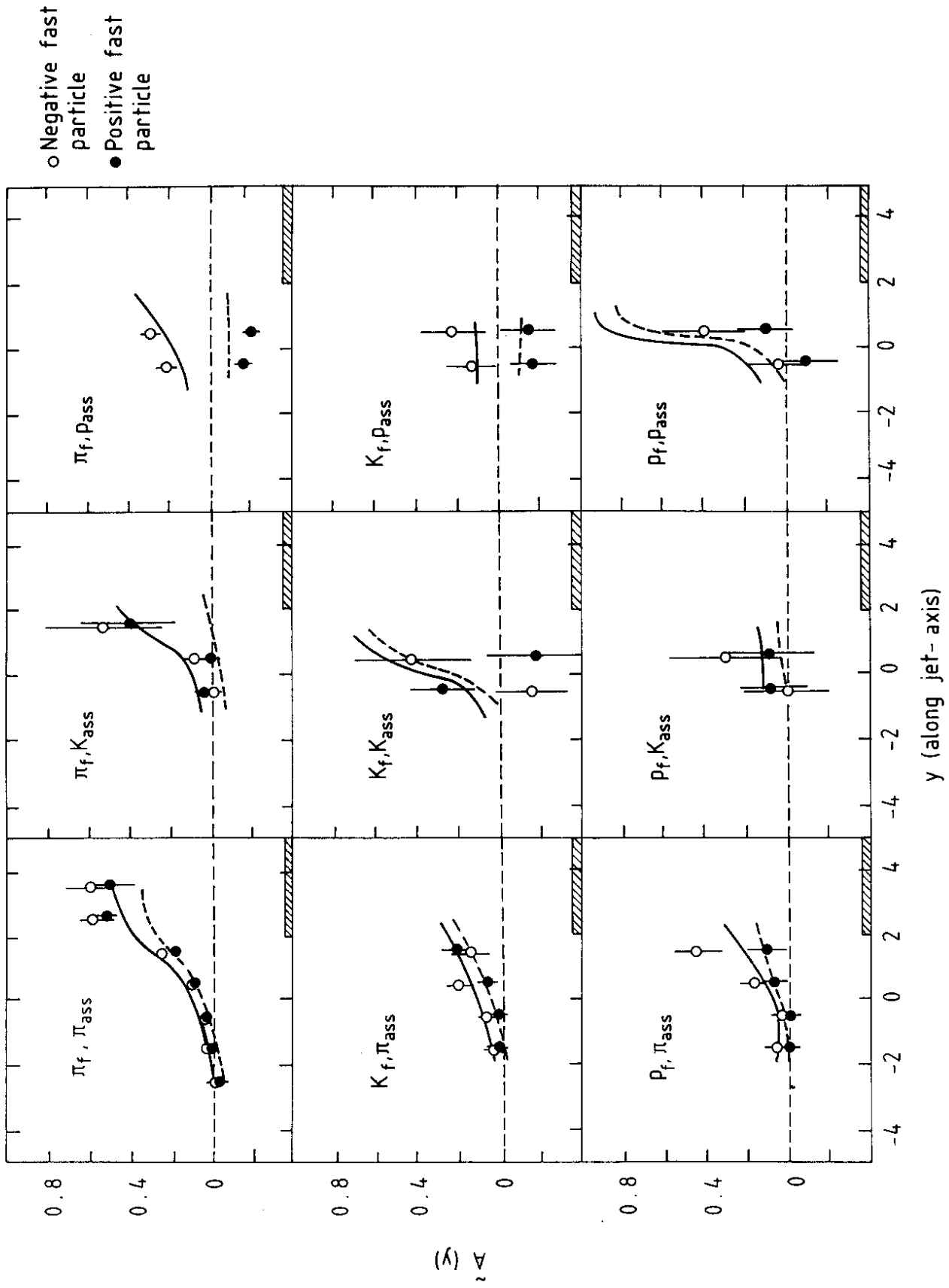
Fig. 11

Fig. 12a

Fig. 12b

Fig. 13